Journal of Applied Electrochemistry
https://doi.org/10.1007/s10800-020-01453-w

RESEARCH ARTICLE

Controlling the ionic polymer/gas interface property of a PEM fuel cell catalyst layer during membrane electrode assembly fabrication

Regis P. Dowd Jr.[1] · **Yuanchao Li**[1] · **Trung Van Nguyen**[1]

Received: 27 August 2019 / Accepted: 19 June 2020

Abstract

During high current density operation, water production in the polymer electrolyte membrane fuel cell (PEMFC) cathode catalyst layer can negatively affect performance by lowering mass transport of oxygen into the cathode. In this paper, a novel heat treatment process for controlling the ionic polymer/gas interface property of the fuel cell catalyst layer is investigated and then incorporated into the membrane electrode assembly (MEA) fabrication process. XPS characterization of the catalyst layer's ionomer-gas interface at its outer surface and its sublayers' surfaces obtained by scraping off successive layers of the catalyst layers confirms that a hydrophobic ionomer interface can be achieved across the catalyst layer using a specific heat treatment condition. Based on the results of the catalyst layer study, the MEA fabrication process is modified to identify heat treatment configuration and conditions that will create an optimal hydrophobic ionomer-gas interface inside the cathode catalyst layer. Finally, fuel cell tests conducted on the conventional and new MEAs under different operating temperatures show the performance of the fuel cells with the treated MEAs was > 130% higher than that with the conventional MEA at 25 °C and 70 °C with humidified air and > 45% higher at 70 °C with dry air. The durability of the hydrophobic treatment on the cathode catalyst layer ionomer is also confirmed by the accelerated stress test.

Graphic abstract

PEMFC Catalyst Layer with Hydrophobic Ionomer/Gas Interface

Electronic supplementary material The online version of this article (https://doi.org/10.1007/s10800-020-01453-w) contains supplementary material, which is available to authorized users.

Extended author information available on the last page of the article

Published online: 30 June 2020

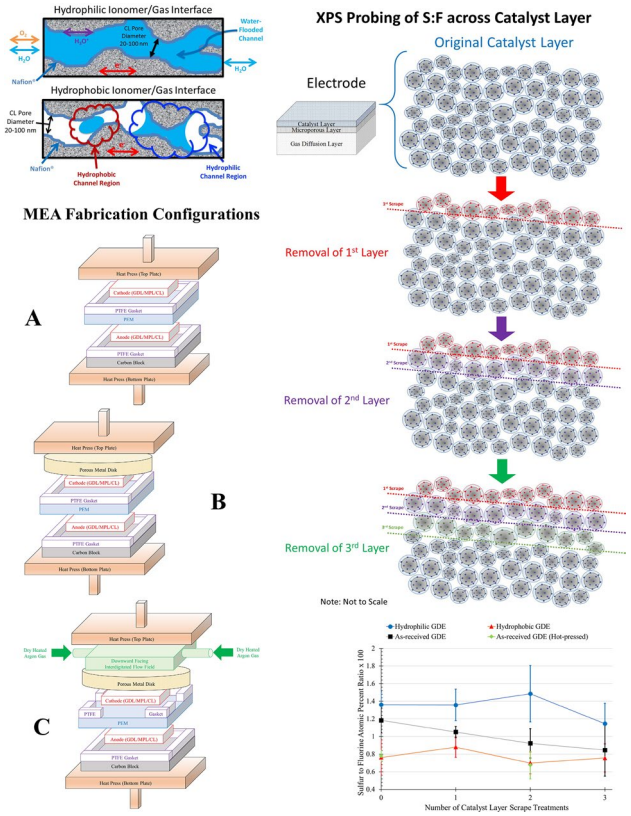

Keywords PEM fuel cells · Catalyst layer · Ionic polymer/gas interface

1 Introduction

The cathode catalyst layer of a polymer electrolyte membrane fuel cell (PEMFC) exhibits high water saturation levels (i.e. flooding conditions) during high current density operations. Water flooding of the cathode results in reduced fuel cell performance due to lower mass transport rate of oxygen to the catalyst reaction site. Various advances have been developed to overcome water management issues related to PEMFCs. A few of these advances include the development of the interdigitated flow field [1], integration of hydrophobic PTFE nanoparticles into the catalyst layer [2, 3], and gas diffusion layer fabrication with various types of non-wetting materials [4, 5], each of these advances led to improved mass transport performance during high current density operations.

The PEMFC catalyst layer is comprised of three phases: an electrically conductive phase (electron transport), an ionically conductive phase (ionic transport), and void spaces to allow for gas/liquid flow. More recently, new analytical techniques such as the X-ray photoelectron spectroscopy (XPS), nano-scale computed tomography, focused ion beam—scanning electron microscopy (FIB-SEM), high-resolution transmission electron microscopy (TEM), cryo-SEM and atomic force microscopy (AFM) have enabled researchers to gain a better understanding of the structure and properties of the PEMFC catalyst layer [6–16], These high-resolution characterization techniques provide scientists additional insight for designing novel catalyst layers to efficiently deliver reactants to and remove products from the electrodes. For example, Litster et.al. was able to use nano-scale computed tomography imaging to probe the fuel cell electrode and generate 3D pore-scale morphological characterizations [13]. FIB-SEM work by Sabharwal et al., high-resolution TEM work by Lopez et al., and cryo-SEM work by Takahashi et al. have enabled improved characterization of the nanostructure and the effect on material properties of the fuel cell CL [14–16].

Typically, a catalyst ink is prepared by mixing carbon powder decorated with catalyst nanoparticles (i.e. Pt), Nafion ionomer, isopropyl alcohol, and water [3, 17–19]. After thorough mixing of the catalyst ink to ensure a homogenous mixture, the catalyst ink is sprayed onto the microporous layer side of a gas diffusion layer for the case of the gas diffusion electrode (GDE), or the membrane for the case of the catalyst coated membrane (CCM). The GDE is then

dried to allow the water and isopropyl alcohol to evaporate, thus leaving behind the catalyst layer. Next, the membrane electrode assembly (MEA) is prepared by hot pressing a proton exchange membrane between two GDEs such that both catalyst layers face the membrane. The MEA is then assembled between two flow fields for delivering the reactants to the cathode and anode.

During the traditional MEA fabrication process, electrodes are hot pressed onto each side of the polymer electrolyte membrane (PEM) such that the catalyst layer side of the electrodes face the membrane. Prior to hot pressing, gaskets with predetermined thicknesses are placed around each electrode to ensure the electrodes are not crushed. Hot pressing is normally completed at 135 °C and 500 kPa above ambient pressure for 5 min [20]. During this process, absorbed water inside the PEM will flash to steam. The steam will diffuse into and saturate the gas pores of the catalyst layer, microporous layer, and gas diffusion layer. With the gaskets surrounding each electrode the steam is prevented from escaping during this process and is only vented when the hot press is disengaged. Since hot pressing is completed above Nafion's glass transition temperature (T_G), the catalyst layer ionomer will bond to the membrane and create a MEA. During the hot-pressing process, ionic pathways are established between the catalyst reaction sites in the catalyst layers of the electrodes and the membrane, which allows ionic conduction from the anode to the cathode during fuel cell operation.

The Nafion ionomer phase in the catalyst layer also undergoes some bulk and interfacial changes during the hot pressing process. Nafion is known to undergo three different relaxations when heated, namely alpha ($\propto$), beta (β) and gamma (γ). The primary $\propto$-relaxation process is the temperature at which larger segments of the polymer become mobile, whereas the sub-glass transition temperature (also called the secondary β-relaxation process) involves localized motion of the polymer backbone and is a precursor to the primary $\propto$-relaxation process [21]. The γ-relaxation process occurs at even lower temperatures and involves localized bond movements (i.e. stretching and bending of bonds). For the purpose of this study, T_G will be used to refer to the primary $\propto$–relaxation process. Nafion has a T_G in the range of 110–130 °C, depending on the degree of hydration and sample aging [22–24]. The dynamic structure of Nafion and dependence on temperature and humidity are well known. Recent work by Kim et al. showed the effect of dispersing solutions and temperature on the properties of Nafion [25]. The surface structural changes of thin film Nafion structures has been shown to depend on the water/vapor environment in contact with Nafion and the annealing conditions [26, 27]. Paul et al. showed how the surface of a 10 nm Nafion thin film switched from hydrophilic to hydrophobic upon thermal annealing and switched back to hydrophilic upon exposure to liquid water [27]. However, our recent work [20] shows that if a controlled cool down process is included during the annealing process to allow the membrane to recrystallize, the surface morphology of the membrane created during annealing could be locked-in. What this means is that if a hydrophobic surface was formed during annealing, the crystallization process will lock-in this surface morphology. Our interpretation of the mechanism to create a hydrophobic ionomer layer in the cathode catalyst layer during hot pressing is described below.

At the onset of MEA hot pressing, a saturated steam environment above glass transition temperature (T_G) created inside the gas pores of the catalyst layer enables the sulfonate ionic groups of the ionomer phase to relax and, therefore, allow reorientation. This reorientation allows the catalyst layer ionomer phase to bond to the membrane and the ionic network in the ionomer layer and on its surface to reorganize. As shown in our previous study [20], a saturated steam environment during annealing and cooling of the MEA will lead to an increased amount of sulfonate ionic groups oriented towards the ionomer/gas interface (inside the gas pores of the catalyst layer) due to their affinity for water. Whereas, a dry gas phase environment during annealing and cooling will result in a lower number of sulfonate ionic groups oriented towards the ionomer-gas interface. As the previous discussion, it's worthy of being addressed again that the outward/inward movement of sulfonic groups can be locked in the recrystallization process (cooling process) by exposing to the saturated/dry gas phase environment to create the hydrophilic/hydrophobic interface. The relative amount of sulfonate ionic groups oriented towards the ionomer/gas interface determines the ionomer's relative hydrophilicity/hydrophobicity. Although the conventional MEA fabrication technique enables the ionomer inside the catalyst layer to form ionic pathways between the catalyst and the membrane, the saturated steam environment inside the gas pores of the catalyst layer while cooling results in a nonhomogeneous ionomer-gas interface (i.e. a mix of hydrophobic and hydrophilic ionomer/gas interfaces). A hydrophobic ionomer-gas interface will minimize liquid water coverage and provide better oxygen gas access to the ionomer phase and catalyst surface. Consequently, an ionomer layer in the catalyst layer with a more uniform and higher fraction of hydrophobic polymer/gas interface will expel liquid water from its surface better and allow greater direct oxygen gas access to the ionomer layer and catalyst active sites.

Based on the concept above, our group envisioned a more ideal and ordered cathode catalyst layer structure that would enable improved two-phase flow (i.e. the gas phase occupies the annular region adjacent to the ionomer/gas interface and water occupies the region along the center of the gas pores). In this inverted annular or liquid-ring flow configuration as highlighted in Fig. 1 [28], oxygen gas transported into the

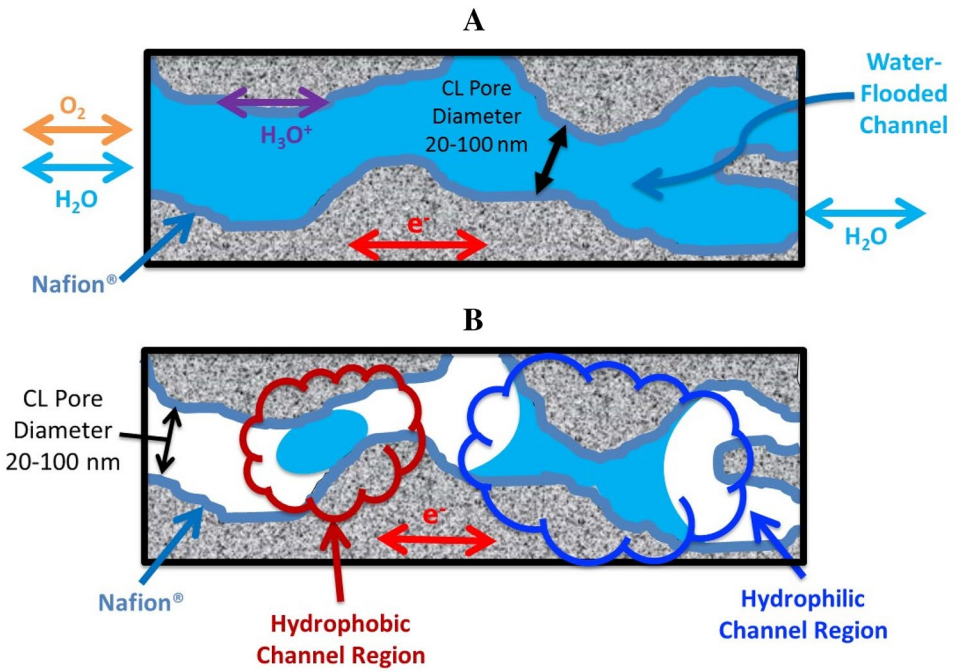

Fig. 1 Cross-sectional side view of **a** water-flooded CL pore and **b** engineered CL ionomer surface [20]

catalyst layer has direct access to the ionomer layer without having to first dissolve in the liquid water phase and diffuse through this barrier in order to reach the ionomer phase. We expected a hydrophobic ionomer/gas interface inside the gas pores of the catalyst layer would lead to higher fuel cell performance during high current density operations due to improved mass transport of oxygen into and water removal from the cathode catalyst layer.

Previously, our research group and others demonstrated this interfacial phenomenon with PFSA membranes [20, 29]. Specific heat treatment conditions led to the formation of either a hydrophobic or hydrophilic membrane surface. This heat treatment technique was then incorporated into the MEA fabrication procedure that resulted in more than a 33% improvement in fuel cell performance [20]. The new MEA fabrication procedure in our previously published work relied on natural convection to remove the steam from the ionomer-gas interface inside the catalyst layer prior to cooling. In this study, a more thorough analysis is completed when applying the heat treatment method to the fuel cell catalyst layer. The catalyst layer's surface is characterized with XPS before and after heat treatment. XPS is also used to characterize the ionomer-gas interface inside the gas pores of the catalyst layer before and after heat treatment. Additionally, a new MEA fabrication technique is explored by using forced convection to remove steam from the catalyst layer during hot pressing. Various forced convection duration times are investigated in order to construct a cathode catalyst layer for optimal two-phase flow. We hypothesize the saturated steam condition at the onset of the MEA fabrication process is required in order to allow the ionomer phase adequate time to relax. Forced convection (i.e. purging with dry heated inert gas) during the final minutes of the MEA fabrication process is expected to remove the saturated steam environment and create a more homogenous hydrophobic ionomer-gas interface. Furthermore, in-depth fuel cell testing is completed to compare the two new MEA fabrication techniques (natural convection and forced convection) with the conventional MEA using various types of flow fields, humidification conditions, and operating temperatures.

2 Experimental

In order to determine if the ionomer/gas interface inside the gas pores of the catalyst layer could be modified to be hydrophobic or hydrophilic, electrodes were exposed to various heat treatment conditions. Sigracet® GDL-25BC carbon electrodes were selected for this purpose. The microporous layer side (MPL) of the gas diffusion electrodes (GDEs) were coated with a Pt/C/Nafion® layer (0.5 mg cm^{-2} Pt geometric area, 0.14 mg cm^{-2} Nafion® ionomer) by TVN Systems Inc. For the hydrophobic case, the GDE was first exposed to a saturated steam environment at a temperature above Nafion's T_G. Then, the saturated steam environment was replaced with heated dry argon gas while maintaining the temperature above Nafion's T_G. Finally, the GDE was allowed to slowly cool to room temperature while maintaining the dry argon environment. For the hydrophilic case, the GDE was first exposed to a saturated steam environment similar to the hydrophobic treated case. After a sufficient

holding time, the saturated steam environment was maintained as the GDE was slowly cooled to room temperature. More specific details on vessel construction and heat treatment conditions can be found in our group's previous work [20].

A Physical Electronics (PHI) VersaProbe II XPS (at Washington University in St. Louis) and VersaProbe III XPS (at University of Kansas) were used to capture high-resolution scans in order to measure the sulfur and fluorine atomic percentages near the catalyst layer's outermost surface. Previously, when analyzing the heat treatment effect on membranes, the sulfur and carbon atomic percentages near the membrane's surface were measured in order to calculate the sulfur to carbon ratio. The sulfur to carbon atomic percent ratio was used to determine the relative hydrophobicity/hydrophilicity of the membrane's surface since a higher amount of sulfonate ionic groups leads to a more hydrophilic skin. However, because of the high carbon content of the catalyst layer, the sulfur to fluorine atomic ratio is used instead to determine the relative amount of hydrophobicity/hydrophilicity of the Nafion ionomer thin film at the catalyst layer's surface.

Next, the catalyst layer side of the heat treated GDEs were lightly scraped with a razor blade to reveal the Nafion ionomer inside the gas pores of the catalyst layer. The CL removal technique enabled removal of the outermost portion to reveal the internal structure of the CL. Further penetration into the CL's internal structure was achieved by additional CL removal steps. XPS depth profiling (i.e. sputtering using argon ion beam etching) was not used because ion beam etching would preferentially remove the ionomer thin film present in the catalyst layer instead of uniformly removing a layer of ionomer and carbon [30]. It is well known that even short sputtering times (< 2 min) can cause rapid degradation to soft materials such as polymers [31–33]. Therefore, low XPS scan times were used to characterize the polymer's surface in order to minimize damage. High-resolution scans at low angle (25°) were collected with the XPS to measure the sulfur and fluorine atomic percentages after each successive removal of a fraction of the catalyst layer. High-resolution scans were collected at multiple locations on each electrode's surface to ensure statistically relevant results. Although XPS probes up to a depth of 3–5 times the inelastic mean free path (IMFP) and the typical IMFP range for polymers is ~ 2–3 nm, the majority of the XPS signal will arise from the first few nanometers of the polymer's surface [15, 34]. Therefore, the sulfur to fluorine atomic percentage trends for the various CL samples can be used to draw conclusions about the ionomer-gas interface. A total of three successive scrapes were used to remove a portion of the catalyst layer to allow the ionomer-gas interface inside the gas pores at various depths of the catalyst layer to be characterized. Figure 2 provides a simplified sketch of how scraping the uppermost surface of the catalyst layer leads to exposure of the ionomer thin film located inside the gas pores of the catalyst layer. After scraping the catalyst layer, XPS was used to characterize the ionomer-gas interface. The ability to characterize the surface and internal ionomer structure for the heat-treated electrodes was important in order to validate that the exposure conditions create a hydrophobic or hydrophilic ionomer-gas interface inside the catalyst layer.

A major purpose of this study was to incorporate the catalyst layer heat treatment exposure conditions into the membrane electrode assembly (MEA) fabrication process. In our previous work, we showed how incorporating a porous metal disk into the MEA fabrication technique, to allow the steam generated during the hot-pressing process to escape, leads to improved mass transport performance during high current density operations [20]. Fuel cells were tested at room temperature and with humidified air flowing to the cathode in order to measure the performance improvement using the new MEA when flooding conditions were present in the cathode. In this paper, we explored more realistic operating conditions in order to maximize fuel cell performance. Therefore, higher temperatures and air humidification levels were investigated.

Traditionally, the MEA is made by hot pressing two electrodes onto each side of a PEM with the catalyst layer side of the electrodes facing the membrane. The traditional MEA hot-pressing setup is shown in Fig. 3a. For this MEA technique, PTFE gaskets are placed around each electrode to ensure the electrodes are not crushed during the hot-pressing procedure. The MEA is hot-pressed at 135 °C and 500 kPa above ambient pressure for 5 min, then removed from the hot-press and allowed to cool to room temperature [35]. In this paper, we explored two new hot-pressing techniques to apply the heat treatment method to the cathode catalyst layer during MEA fabrication. Both new methods intended to recreate the conditions necessary to create a hydrophobic ionomer-gas interface inside the gas pores of the catalyst layer. A hydrophobic ionomer-gas interface in the cathode catalyst layer of a H_2-air PEMFC is expected to result in improved gas and liquid transport into and out of the catalyst layer, respectively.

First, natural convection was explored by inserting a porous metal disk (stainless steel 2″ diameter, 0.062″ thick, 100-micron average pore size) above the cathode. For the natural convection setup, Fig. 3b, a porous metal disk was placed above the cathode to allow a pathway for steam to escape. During hot pressing, moisture in the PEM flashes to steam and creates a saturated steam environment inside the gas pores of the catalyst layer. By inserting a porous metal disk above the cathode, the steam concentration gradient created between the pores of the catalyst layer and pores of the metal disk enables natural convection of steam out of the catalyst layer to occur. The natural convection setup

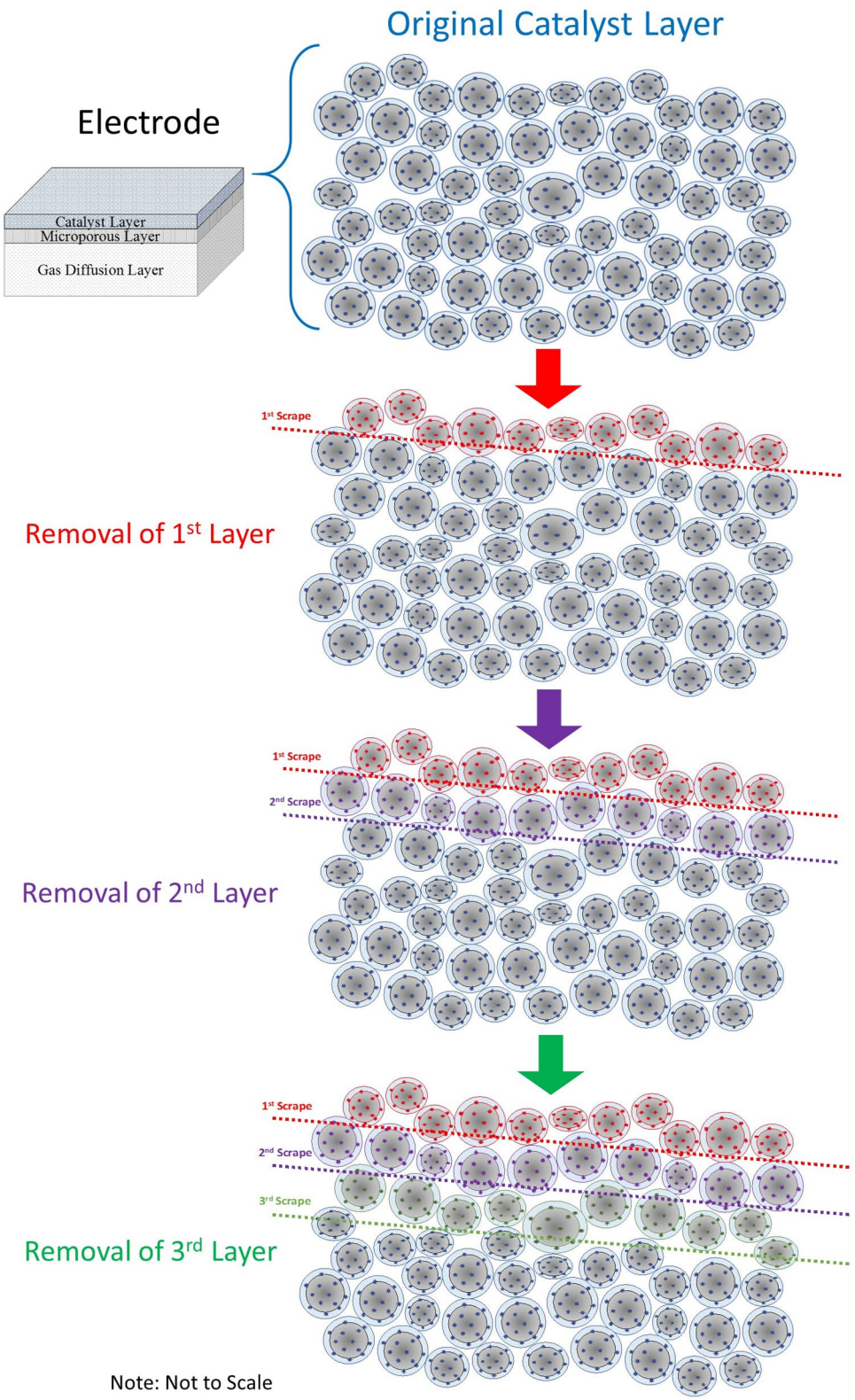

Fig. 2 Layer by layer removal process of catalyst layer for XPS analysis

allows steam to escape radially out through the porous metal disk. Another natural convention configuration that is possible but was not investigated in this study is to use a gasket with channels cut (i.e., incomplete gasket) in the gasket to allow steam to escape radially from the electrode during hot pressing [36].

Next, forced convection was investigated by inserting an interdigitated carbon flow field face down above the porous

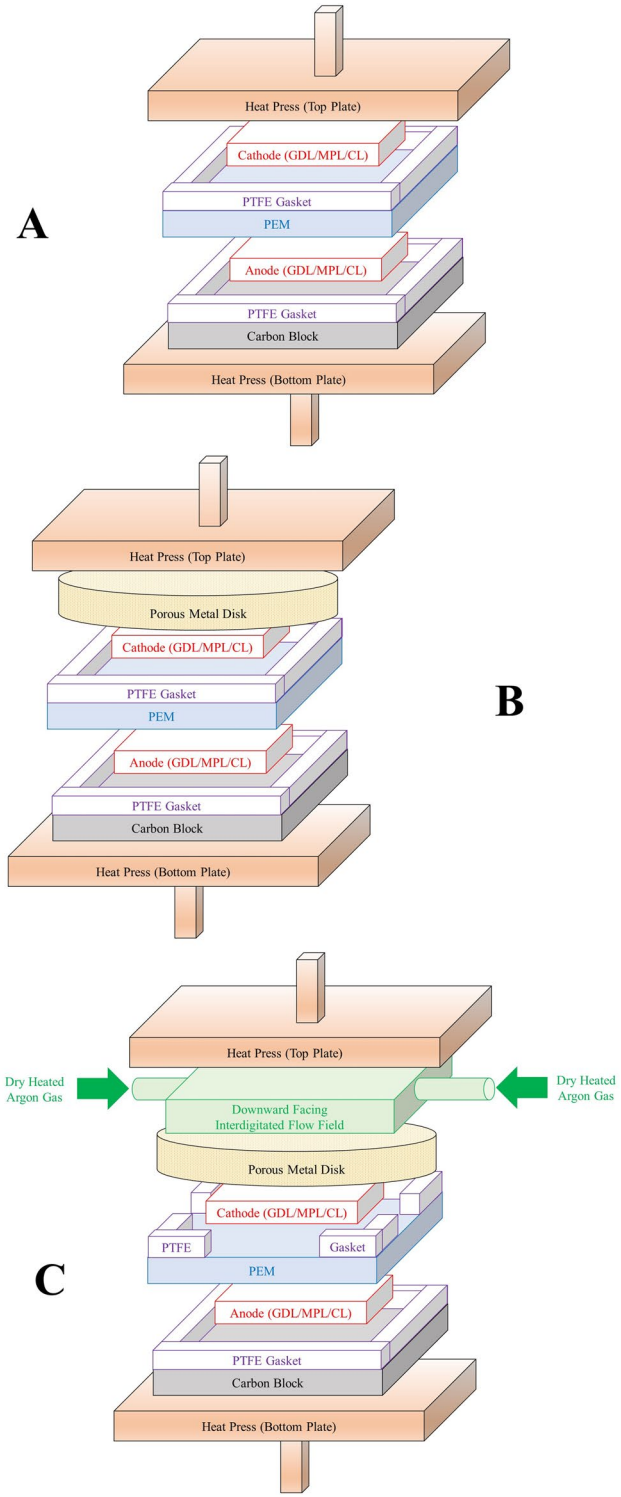

Fig. 3 MEA hot-press setup for (**a**) normal MEA, (**b**) natural convection MEA and (**c**) forced convection MEA

metal disk and flowing dry heated argon gas during the MEA fabrication process. The dry heated argon gas was directed simultaneously into the inlet and outlet of the interdigitated carbon flow field such that argon flowed down through the porous metal disk and cathode. For the forced convection setup, channels were cut into the gasket surrounding the cathode in order to provide a pathway for heated dry argon to flow through the electrode during hot pressing. The heated argon was able to vent out from both the edges of the porous metal disk and the edges of the cathode. Noted that the forced convection configuration is actually a combination of natural convection and forced convection because prior to the introduction of heated gas, it is identical to the natural convection configuration. The forced convection setup is shown in Fig. 3c.

For the forced convection setup, flow duration was investigated to determine the effect on fuel cell performance. The following forced convection MEAs were tested: 5 min of forced convection during the entire hot-pressing procedure, 3 min no flow followed by 2 min of forced convection, and 4 min no flow followed by 1 min of forced convection. The MEAs were then removed from the hot-press and allowed to cool to room temperature in ambient environment. We hypothesized that there would be an optimal flow duration which would result in peak fuel cell performance. Our hypothesis required an initially saturated steam environment for sufficient duration in order to provide adequate time for the ionomer to relax. A steam environment inside the gas pores of the catalyst layer would enable the ionomer phase to relax and allow the sulfonate ionic groups within the Nafion ionomer to reorient themselves. Next, as dry heated argon flowed through the gas pores of the catalyst layer and steam was removed, the sulfonate ionic groups were expected to reorient themselves and migrate inward towards any remaining moisture inside the bulk of the ionomer. This leads to a hydrophobic ionomer-gas interface due to an ionomer-gas surface rich in fluorinated-carbon backbone structure and void of sulfonate ionic groups.

For PEMFC testing, discharge polarization curves were collected at various fuel cell temperatures and air humidification conditions using MEAs prepared with the procedure outlined in the paragraph above. Two studies were conducted using the following temperature and humidification conditions: (a) Fuel cell at 25 °C, H_2 humidification bottle at 25 °C, Air humidification bottle at 25 °C; (b) Fuel cell at 70 °C, H_2 humidification bottle at 95 °C, Air humidification bottle at 70 °C or Dry Air at 70 °C. A higher humidification temperature 95 °C is used for the hydrogen gas to inject more water into the hydrogen side to prevent it from drying out during discharge operation [37–39]. With the fuel cell maintained at a lower temperature (70 °C) than the H_2 humidification bottle, the excess water vapour will condense and be carried into the hydrogen electrode to provide additional water to compensate for the amount lost in the anode due to electroosmotic drag by the transport of protons from the anode to cathode during discharge operation.

This two-phase water humidification approach was used by Wood and Nguyen in their study [38]. Table 1 lists the key parameters used for each fuel cell study.

All fuel cell testing was completed using a hydrogen pressure of 0.136 MPa (5 psig) and flow rate of approximately 660 mL min^{-1} (Equivalence of 51.7 A cm^{-2}) by using a recirculation pump. Air was delivered to the cathode at a rate of approximately 350 mL min^{-1} (Equivalence of 8.6 A cm^{-2}) in a flow-through setup. Nafion 212 (~ 51 µm thick) was used for the polymer electrolyte membrane for all MEAs and electrical current was collected from the edges of the current collectors. Sigracet GDL-25BC carbon electrodes were used as the substrates for both the hydrogen and air electrodes. A catalyst layer (0.5 mg cm^{-2} Pt geometric area, 0.14 mg cm^{-2} Nafion ionomer) was spray coated onto the microporous layer side of the GDLs. A start-up procedure consisted of operating each PEMFC at 0.2 V until 0.4 A cm^{-2} was achieved, then holding the discharge current steady at 0.4 A cm^{-2} for 1 h [35]. The standardized start-up procedure ensured all MEAs were conditioned (i.e. hydrated) properly prior to collecting discharge polarization curves. Discharge polarization curves were collected by using constant voltage staircases in 50 mV increments from OCV to 0.2 V. Multiple discharge polarization curves were collected for each MEA to ensure repeatable results. EIS was completed at 5 mV amplitude over a frequency range of 1 Hz to 100 kHz on each fuel cell to measure the internal cell resistance. EIS was also completed on the fuel cell fixture without a MEA to measure the electrical resistance of the fuel cell components.

The MEA with 1-min forced convection was selected for the accelerated stress test (AST) to check the durability of the catalyst layer treatment, during which the combination of the interdigitated flow field, 90 °C humidified H_2, and 70 °C humidified air was used as the fuel cell operating conditions. Before the AST, the discharge polarization curve was collected following the procedure described above. The AST was conducted based on the protocol of the Department of Energy [40]. The voltage was cycled between 30 s at 0.9 V and 30 s at 0.7 V. After 1200 cycles, another discharge polarization curve was collected.

3 Results and discussion

After exposing several catalyst-coated GDEs to various heat treatment conditions, XPS was used to validate that the exposure conditions created a hydrophobic or hydrophilic ionomer-gas interface on the surface and inside the gas pores of the catalyst layer. Figure 4 shows the sulfur to fluorine ratio for the hydrophilic-treated, hydrophobic-treated, and as-received GDEs. Each point represents an average of three to five measurements. The original XPS spectra and sulfur to fluorine ratios are included in Fig. S1 through Fig. S4 and Table S1 through Table S4, respectively. Figure 4 also includes results for as-received GDEs (TVN Systems, Inc.) after hot-pressing them between two carbon plates (without a gasket around the GDE). This process is similar to the natural convection process with the porous metal plate described earlier in Fig. 3b. The sulfur to fluorine ratio at point 0 (far-left points in Fig. 4) corresponds to the outermost surface of the catalyst layer prior to applying the scraping procedure. As expected, the hydrophilic-treated GDE had a higher sulfur to fluorine ratio compared to the as-received, as-received and hot-pressed, and hydrophobic-treated GDEs. It is not surprising that the S:F ratio for the

Table 1 Experimental studies and conditions

Study #	1	2
Experimental variable	Temperature	Air humidification
MEA type	Normal MEA	Same
	Natural convection MEA	
	Forced convection MEA	
Cathode	SGL 25BC GDL coated with Pt/C/Nafion layer (0.50 mg-Pt cm^{-2}, 0.14 mg cm^{-2} Nafion ionomer)	Same
Anode	SGL 25BC GDL coated with Pt/C/Nafion layer (0.50 mg-Pt cm^{-2}, 0.14 mg cm^{-2} Nafion ionomer)	Same
Membrane	NR212	Same
Flow fields	Interdigitated carbon flow fields	Same
Air flow rate	350 mL min^{-1}	Same
H_2 flow rate and pressure	660 mL min^{-1} & 0.136 MPa	Same
Temperature	25 °C fuel cell, hydrogen, & air	70 °C fuel cell & air, 95 °C hydrogen
	70 °C fuel cell & air, 95 °C hydrogen	
Humidification	Humidified hydrogen and air	Humidified hydrogen & dry air

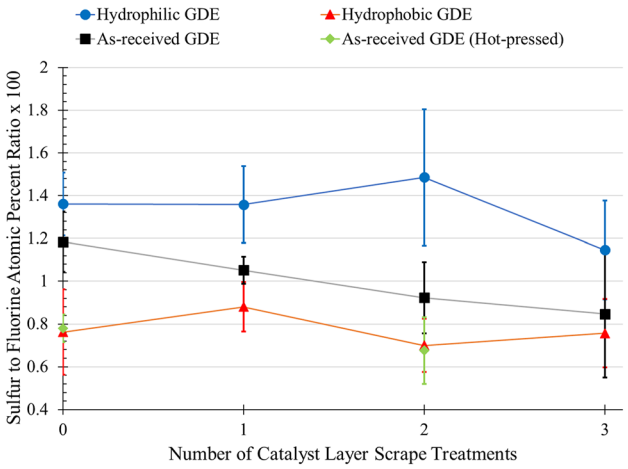

Fig. 4 XPS characterization of catalyst layer

as-received GDE is between those of the hydrophilic and hydrophobic GDEs. The same result was observed in our earlier work with Nafion membranes [20]. What is new and interesting is that the sulfur to fluorine ratio of the as-received GDE hot-pressed in a natural convection mode is similar to that of the hydrophobic GDE. The hot-pressed data points (green/diamond symbols in Fig. 4) were obtained after the fuel cell tests were completed because we were curious about the performance of the natural convection MEA.

After scraping each GDE (to expose the ionomer-gas interface inside the gas pores of the catalyst layer), XPS was used to measure the sulfur to fluorine ratio. The magnitude and trend of the sulfur to fluorine ratio after each successive scrape (to remove a portion of the catalyst layer) continued throughout the catalyst layer for both heat treatment conditions and the as-received GDE. The calculated sulfur to fluorine atomic percent ratio for a 1100 equivalent weight Nafion membrane is approximately 2.5%. The sulfur to fluorine ratio for all data in Fig. 4 is below 1.5%. During exposure to x-ray radiation for XPS measurements, it is well known that Nafion's surface will experience preferential removal of sulfur compared to other atoms (i.e. fluorine, carbon) due to lower bond strength. The XPS settings (i.e. beam power and measurement duration) are important for ensuring a reliable sulfur signal and minimizing removal of sulfur atoms. Therefore, only the trends and the relative comparison between the three curves in Fig. 4 can be relied upon, not the actual values. These results support our hypothesis that specific heat treatment conditions can create a hydrophilic or hydrophobic ionomer-gas interface for the thin ionomer film on the surface and inside the catalyst layer.

Next, MEAs were constructed using the normal (i.e. conventional method), natural convection, and forced convection MEA procedures. The MEAs were tested at various

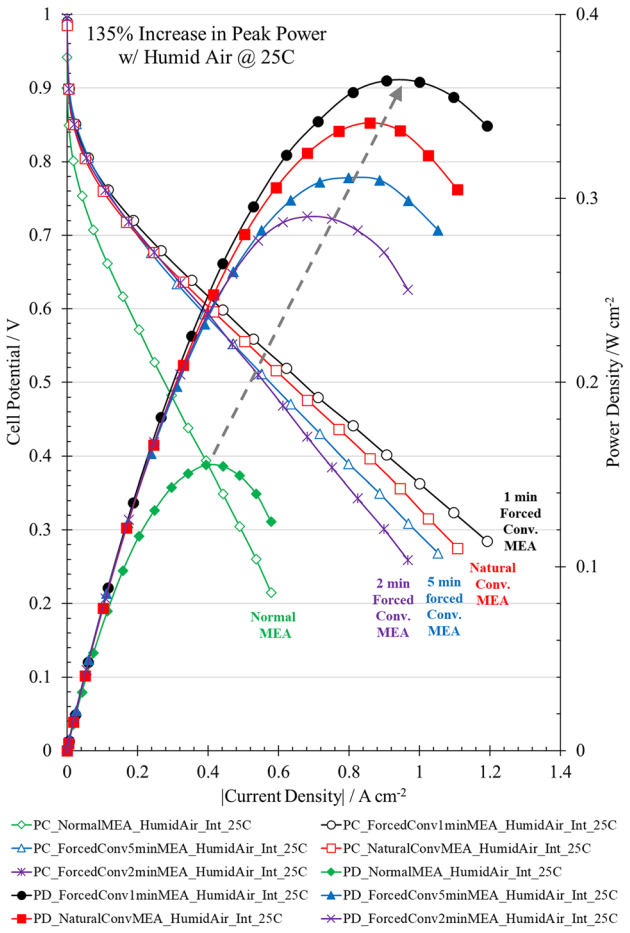

Fig. 5 H_2-Air PEMFC discharge polarization and power density curves for normal, natural and forced convection MEAs with different purge times at 25 °C using humidified hydrogen and humidified air

temperatures and air humidification conditions. The 25 °C results of the fuel cells with the five MEAs made with the three different hot-pressing configurations are given in Fig. 5. As shown in this figure, the fuel cell with the normal MEA performed poorly at 25 °C under water saturated air condition (as expected) because the cathode was probably flooded or partially flooded over most if not all of the current density range, even at low current densities. Its peak power density is only 155 mW cm^{-2}. Note that if the cathode inlet air is already saturated with water vapor, then any water that is generated in the cathode catalyst layer would very likely remain as liquid water. Therefore, a catalyst layer that is not designed to handle high liquid water saturation (i.e. normal MEA) would very likely be flooded. Excessive flooding of the catalyst layer can affect the fuel cell performance even at low current densities by making a significant fraction of the catalyst region in the catalyst layer inaccessible.

Meanwhile, the fuel cells with treated MEAs to create a more hydrophobic Nafion ionomer/gas interface performed much better than the normal MEAs over the entire current

density range. The order of performance (from high to low) for these treated MEAs at 25 °C with water saturated air was 1-min forced convection, natural convection, 5-min forced convection, and 2-min forced convection with the peak power density ranging from 364 mW cm^{-2} for the MEA with 1-min of forced convection to 290 mW cm^{-2} for the 2-min forced conventional MEA. The performance of the 1-min forced convection MEA is 135% better than that of the normal MEA. Its performance was better than those of the other three treated MEAs over the entire current density range, evidence of having better oxygen gas access and mass transport property. The performance of the other three treated MEAs was similar in the kinetic controlled, low current density range and only differed in the high current density, mass controlled region where liquid coverage of the Nafion ionomer layer plays a crucial role. From these results, one could infer that these three MEAs had similar effective active surface areas but slightly different oxygen gas access and mass transport properties.

The performance of the natural convection MEA is interesting. Its polarization curve was almost parallel to that of the 1-min forced convection case, and its peak power density was the second best at 339 mW cm^{-2}. The main difference between these two cases are the use of the porous metal plate to allow steam to escape in the natural convection case versus the cut channels in the forced convection case during this first four minutes of the hot pressing process and use of forced convection to purge steam from the electrode during the last minute of the forced convection case. Having the porous metal plate over the whole electrode may allow more steam to escape from the.

whole electrode than from the edges of the electrode through some of the cut channels. From the differences in their configurations, it could be inferred that the 1-min forced convection case allowed slower steam venting in the first four minutes and therefore more time for the polymer to relax and form a good ionic network within the polymer and with the catalyst surface, and its 1-min of forced venting with heated gas allows the formation of a higher level of hydrophobic ionomer film/gas interface in the catalyst layer. Our hypothesis stated that sufficient time is needed at saturated steam conditions (above Nafion's T_G) to allow the ionomer layer to relax and the sulfonate ionic groups to be able to reorient themselves. We believe these two characteristics gave the 1-min forced convection MEA better liquid water handling capability in the catalyst layer. The lower performance of the MEAs in the 2-min and 5-min forced convection cases could be attributed to the Nafion membrane and ionomer layer not having sufficient relaxation time to form a good ionic network within the polymer and the ionic clusters. The treated MEA results show that more time for membrane relaxation was needed and one minute of argon purging was sufficient to purge most of the moisture from the catalyst layer to create a hydrophobic ionomer/gas interface.

The fuel cell test results of the five different MEAs at 70 °C under water-saturated air inlet condition are shown in Fig. 6. At 70 °C, where the transport rate of oxygen and the kinetic rate of oxygen reduction are higher, all MEAs performed better (as expected) with power densities about 100% higher than those at 25 °C. As in the 25 °C case, a similar order in performance was observed with the 1-min forced convection MEA having the best performance with peak power of 763 mW cm^{-2} and the normal MEA with the lowest performance with peak power of 327 mW cm^{-2}. This 133% difference in performance is very similar to the 135% difference observed at 25 °C under saturated air conditions. The polarization curves for the treated MEAs at this temperature are similar to those at 25 °C. The 1-min forced convection MEA performed better than those of the other three treated MEAs over the entire current density range. The polarization curves of the three treated MEAs

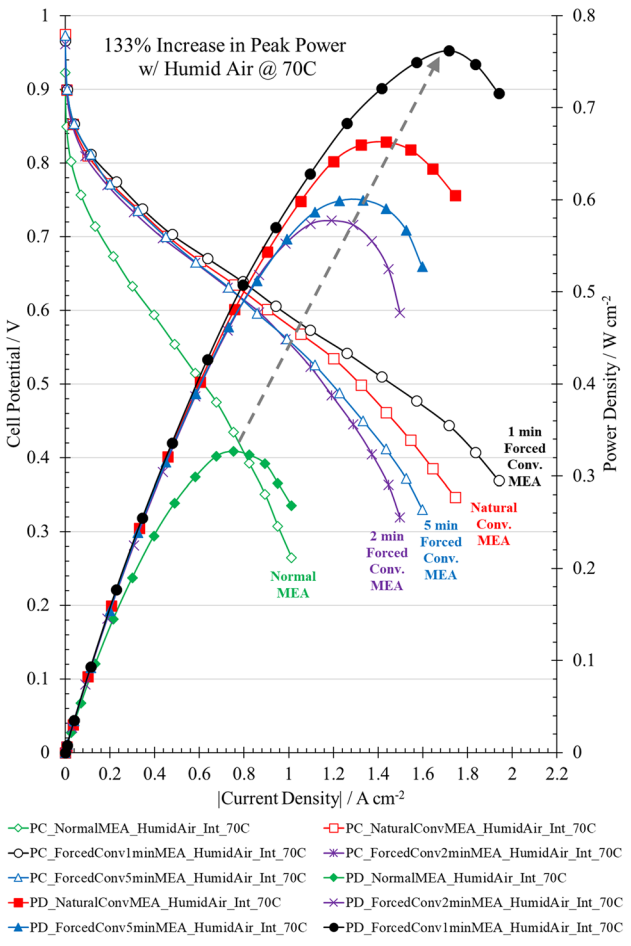

Fig. 6 H_2-Air PEMFC discharge polarization and power density curves for normal MEA, natural convection MEA, and forced convection MEAs with different purge times at 70 °C using humidified hydrogen and humidified air

were similar in the low current density range and only differed in the mass-transfer controlled, high current density region. The fuel cell peak power densities for all MEAs at 25 °C and 70 °C under water vapor saturated inlet air conditions are summarized in Table 2.

Lastly, the MEAs made by various hot-pressing methods were tested using dry air instead of humidified air. It is well known that flowing dry air to the cathode will lead to higher performance due to improved liquid water removal, mass transport of oxygen, and higher oxygen concentration in the gas phase [37, 38]. Dry air is better able to remove liquid water from the cathode, therefore reducing the impact of liquid water buildup and enabling better oxygen transport into the cathode to reach the catalyst reaction sites. The results for the dry air 70 °C tests given in Fig. 7 show current density higher than 2 A cm^{-2} and peak power density greater than 800 mW cm^{-2} were achieved with dry air. The normal MEA, which did not perform well under water saturated air, was able to achieve a current density of more than 1 A cm^{-2} at 0.5 V and peak power of 550 mW cm^{-2}, which are in alignment with previously published results using state-of-the-art fuel cells at similar operating conditions [19, 38, 41–44]. The peak power density of the normal MEA increased the most, by 68%, when dry air was used instead of water saturated air while those of the treated MEAs only increased by 4–12%. The peak power of the best performing 1-min forced convection MEA is now only 47% higher than that of the normal MEA as compared to the ~ 130% difference observed under water saturated condition. See the peak power comparisons given in Table 1. The 70 °C with dry air test results show that the dry air condition primarily benefited the MEA that did not handle saturated liquid water conditions well (e.g. "normal" MEA). The MEAs able to handle high liquid water saturation condition well (e.g. the treated MEAs) did not benefit as much by the dry air condition. However, the treated MEAs show that with improved water saturation handling capability, they can operate in both low and high humidity air conditions and

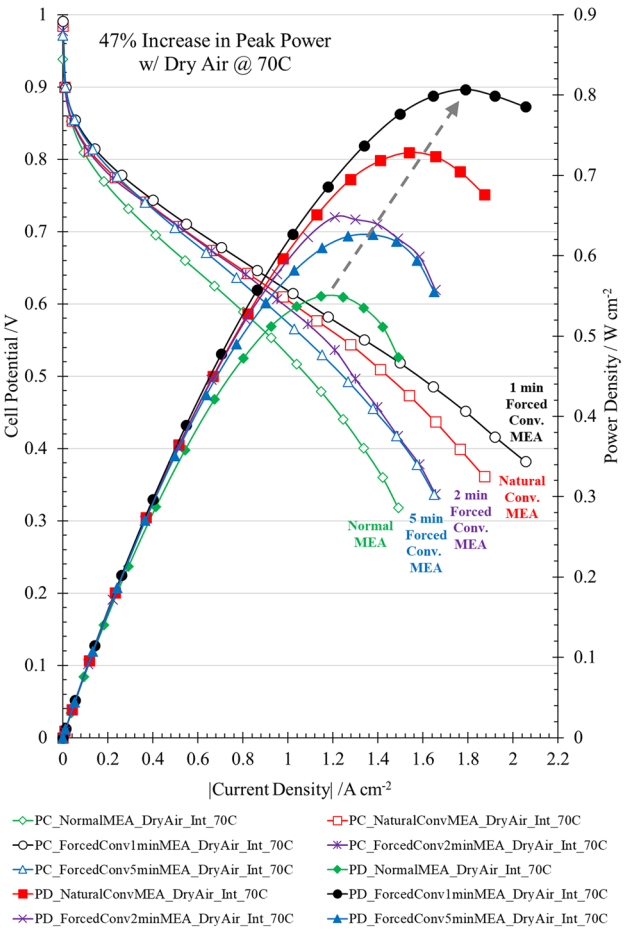

Fig. 7 H_2-Air PEMFC discharge polarization and power density curves for normal MEA, natural convection MEA, and forced convection MEAs with different purge times at 70 °C using humidified hydrogen and dry air

at high current densities when high liquid water saturation level in the catalyst layer is expected.

The AST test results in Fig. 8a show that the current densities decrease by 1.7% (at 0.9 V) and 5.1% (at 0.7 V) respectively. This is lower than the typical degradation of

Table 2 Peak power density achieved by the five different MEAs

Peak power density (mW cm^{-2})			
	Temperature		
MEA	Case 1 (25 °C-Humidified air)	Case 2 (70 °C-Humified air)	Case 3 (70 °C-Dry air)
Normal	155	327 (111%)	550 (255%)* (68%)**
Natural convection	339	663 (96%)	728 (115%)* (10%)**
1-min forced convection	364	763 (110%)	807 (122%)* (6%)**
2-min forced convection	290	577 (99%)	648 (123%)* 12 (%)**
5-min forced convection	311	600 (93%)	626 (101%)* (4%)**

*Percent increase over case 1

**Percent increase over case 2

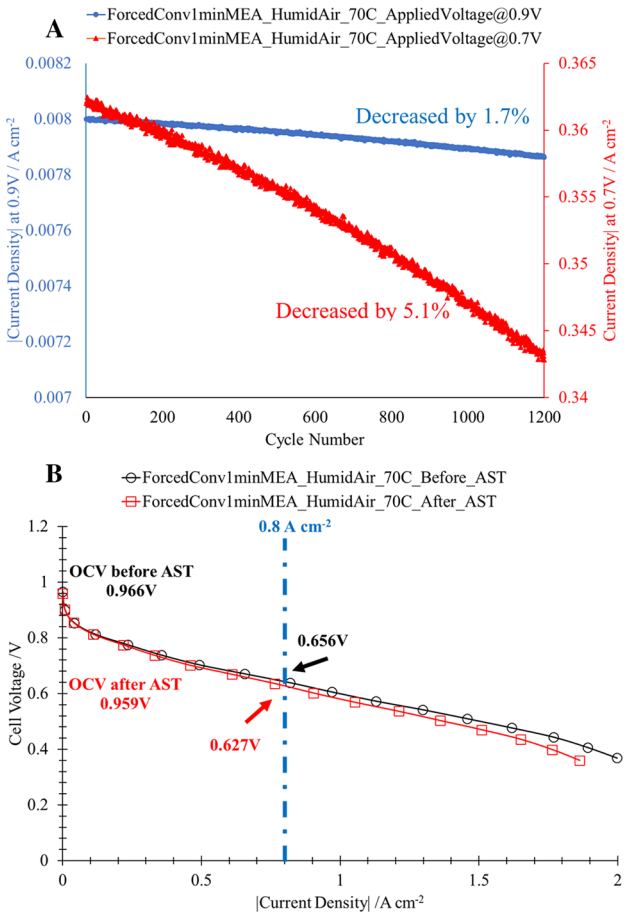

Fig. 8 Results of accelerated stress test (AST) for the MEA with the 1-min forced convection at 70 °C using humidified hydrogen and air. (**a**) Current densities of applied voltage at 0.9 V (blue curve with circle markers) and 0.7 V (red curve with triangle markers) during AST, (**b**) H_2-Air PEMFC discharge polarization curves before and after AST

catalyst on a support, which has been reported to drop 13.8% in normalized ECSA after 1000 cycles of AST [45]. The discharge curves before and after AST given in Fig. 8b show that the OCV decreases from 0.966 to 0.959 V (−7 mV), while the voltage at 0.8 A cm^{-2} decreases from 0.656 to 0.627 V (−29 mV). Moreover, the high mass transfer resistance caused by water flooding in the catalyst layer of the normal MEA (green/diamond symbols in Fig. 7) is still avoided after AST cycles, which confirms that the hydrophobic treatment on the ionomer of the catalyst layer has a good durability effect.

4 Conclusions

In summary, a new heat treatment process was developed and used to create a hydrophobic ionomer/gas interface in a fuel cell catalyst layer. The XPS characterization results of the surface and different sublayers of the catalyst layer of the gas diffusion electrode confirmed that a hydrophobic ionomer interface was achieved across the catalyst layer. Based on these results, new MEA fabrication configurations and procedures that allow natural and forced venting of the steam generated in the MEA during hot pressing were developed. These configurations were used to identify heat treatment configurations and exposure conditions that would create an optimal hydrophobic ionomer-gas interface inside the cathode catalyst layer.

The fuel cell tests conducted on the untreated and treated MEAs under different operating temperatures show the treated MEAs had better liquid water saturation handling properties and better fuel cell performance especially under high water saturation conditions (e.g. operation with water-saturated air). The best fuel cell performance was achieved with the MEA fabricated by the forced convection configuration with 1-min forced venting. Its peak power density at 25 °C and 70 °C under water saturated air condition was greater than 130% higher than that of the MEA made by the conventional hot-pressing method. At 70 °C operating condition, when dry air was used, the conventional MEA, that had shown poorer performance under water saturated air condition because of its poorer liquid water saturation handling capability, benefited the most. Its power density increased more than 68% from 327 to 550 mW cm^{-2}, while the treated MEAs with improved liquid water handling capability only increased about 4–12%. The best performance achieved under dry air condition was obtained with the 1-min forced convection MEA with a peak power density of 807 mW cm^{-2}. Its long-term durability and stability was confirmed by accelerated stress testing, which showed low mass transfer resistance in the high current density region. Finally, the treated MEA results show that in the newly developed MEA hot-pressing techniques, the two most important variables are the polymer relaxation time and the venting time.

Acknowledgements Regis Dowd Jr. wishes to acknowledge the financial support from the University of Kansas (KU) Madison and Lila Self Fellowship. The authors would like to thank Dr. Prem Thapa at the University of Kansas and Dr. Vijay Ramani, Dr. Huafang Li, and Yue Li at Washington University in St. Louis for their support and expertise in using the XPS. The authors would also like to thank Applied Porous Technologies, Inc. for providing the porous stainless-steel disk used for MEA fabrication. This work was also supported by the National Science Foundation under Grant Numbers EFRI-1038234 and CBET-1518755/1803058.

Author contributions The research was done by RPD under the direction of TVN. The manuscript was written by both RPD and TVN. YL conducted additional experiments to obtain the results in Figs. 4 and 8 and provided additional analysis of these results.

Compliance with ethical standards

Conflict of interest The authors declare that the research was conducted in the absence of any commercial or financial relationships that could be construed as a potential conflict of interest.

Contribution to the field statement During high current density operation, liquid water production in the polymer electrolyte membrane fuel cell cathode catalyst layer can negatively affect performance by lowering mass transport of oxygen into the cathode. In this paper, a novel heat treatment process for making the ionic polymer/gas interface of the fuel cell catalyst layer hydrophobic is incorporated into the membrane electrode assembly (MEA) fabrication process. The hydrophobic ionomer layer interface helps to keep the ionomer free of liquid water and therefore more accessible to oxygen gas. It also helps to expel water more rapidly from the gas pores in the catalyst layer. Fuel cell test results of MEAs fabricated by this process show improved performance compared to conventional MEAs, especially under high water saturation operating conditions. The fuel cell performance of the treated MEA was > 130% better than the conventional MEA at both 25 °C and 70 °C when supplying humidified air and > 45% better at 70 °C with dry air.

References

1. Nguyen TV (1996) A gas distributor design for proton-exchange-membrane fuel cells. J Electrochem Soc 143(L103):L105. https://doi.org/10.1149/1.1836666
2. Friedmann R, Nguyen TV (2010) Optimization of the microstructure of the cathode catalyst layer of a PEMFC for two-phase flow. J Electrochem Soc 157:B260. https://doi.org/10.1149/1.3264628
3. Uchida M (1995) Investigation of the microstructure in the catalyst layer and effects of both perfluorosulfonate ionomer and PTFE-loaded carbon on the catalyst layer of polymer electrolyte fuel cells. J Electrochem Soc 142:4143. https://doi.org/10.1149/1.2048477
4. Benziger J, Nehlsen J, Blackwell D, Brennan T, Itescu J (2005) Water flow in the gas diffusion layer of PEM fuel cells. J Membrane Sci 261:98–106. https://doi.org/10.1016/j.memsci.2005.03.049
5. Nguyen TV, Ahosseini A, Wang X, Yarlagadda V, Kwong A, Weber AZ, Deevanhxay P, Tsushima S, Hirai S (2015) Hydrophobic gas-diffusion media for polymer-electrolyte fuel cells by direct fluorination. J Electrochem Soc 162:F1451–F1460. https://doi.org/10.1149/2.0411514jes
6. Dowd RP, Nguyen TV, Moore DS, Pintauro PN, Park JW (2013) Conductive AFM study to differentiate between the surface ionic conductivity of nafion and electrospun membranes. ECS Trans 58:607–613. https://doi.org/10.1149/05801.0607ecst
7. Nguyen TV, Nguyen MV, Lin G, Rao N, Xie X, Zhu D-M (2006) Characterization of surface ionic activity of proton conductive membranes by conductive atomic force microscopy. Electrochem Solid-state Lett 9:A88–A91. https://doi.org/10.1149/1.2154328
8. Nguyen TV, Nguyen MV, Nordheden KJ, He W (2007) Effect of bulk and surface treatments on the surface ionic activity of nafion membranes. J Electrochem Soc 154:A1073. https://doi.org/10.1149/1.2781247
9. Ferreira-Aparicio P, Gallardo-Lopez B, Chaparro A, Daza L (2011) Physico-chemical study of the degradation of membrane-electrode assemblies in a proton exchange membrane fuel cell stack. J Power Sources 196:4242–4250. https://doi.org/10.1016/j.jpowsour.2010.10.059
10. Paul DK, Karan K, Docoslis A, Giorgi JB, Pearce J (2013) Characteristics of self-assembled ultrathin Nafion films. Macromolecules 46:3461–3475. https://doi.org/10.1021/ma4002319
11. Zamel N (2016) The catalyst layer and its dimensionality–A look into its ingredients and how to characterize their effects. J Power Sources 309:141–159. https://doi.org/10.1016/j.jpowsour.2016.01.091
12. Zhang F-Y, Advani SG, Prasad AK, Boggs ME, Sullivan SP, Beebe T (2009) Quantitative characterization of catalyst layer degradation in PEM fuel cells by X-ray photoelectron spectroscopy. Electrochim Acta 54:4025–4030. https://doi.org/10.1016/j.electacta.2009.02.028
13. Litster S, Epting W, Wargo E, Kalidindi S, Kumbur E (2013) Morphological analyses of polymer electrolyte fuel cell electrodes with nano-scale computed tomography imaging. Fuel Cells 13:935–945. https://doi.org/10.1002/fuce.201300008
14. Sabharwal M, Pant L, Putz A, Susac D, Jankovic J, Secanell M (2016) Analysis of catalyst layer microstructures: from imaging to performance. Fuel Cells 16:734–753. https://doi.org/10.1002/fuce.201600008
15. Lopez-Haro M, Guétaz L, Printemps T, Morin A, Escribano S, Jouneau P-H, Bayle-Guillemaud P, Chandezon F, Gebel G (2014) Three-dimensional analysis of Nafion layers in fuel cell electrodes. Nat Commun 5:1–6. https://doi.org/10.1038/ncomms6229
16. Takahashi S, Mashio T, Horibe N, Akizuki K, Ohma A (2015) Analysis of the microstructure formation process and its influence on the performance of polymer electrolyte fuel-cell catalyst layers. ChemElectroChem 2:1560–1567. https://doi.org/10.1002/celc.201500131
17. Qi Z, Kaufman A (2002) Improvement of water management by a microporous sublayer for PEM fuel cells. J Power Sources 109:38–46. https://doi.org/10.1016/S0378-7753(02)00058-7
18. Antolini E, Giorgi L, Pozio A, Passalacqua E (1999) Influence of Nafion loading in the catalyst layer of gas-diffusion electrodes for PEFC. J Power Sources 77:136–142. https://doi.org/10.1016/S0378-7753(98)00186-4
19. Mack F, Klages M, Scholta J, Jörissen L, Morawietz T, Hiesgen R, Kramer D, Zeis R (2014) Morphology studies on high-temperature polymer electrolyte membrane fuel cell electrodes. J Power Sources 255:431–438. https://doi.org/10.1016/j.jpowsour.2014.01.032
20. Dowd RP, Day CS, Nguyen TV (2016) Engineering the ionic polymer phase surface properties of a pem fuel cell catalyst layer. J Electrochem Soc 164:F138–F146. https://doi.org/10.1149/2.1081702jes
21. Smith GD, Bedrov D (2007) Relationship between the α-and β-relaxation processes in amorphous polymers: Insight from atomistic molecular dynamics simulations of 1, 4-polybutadiene melts and blends. J Poly Sci Part B: Poly Phys 45:627–643. https://doi.org/10.1002/polb.21064
22. Colak O, Acar A, Ergenekon E (2013) Investigation of hygro-thermal cycle effects on the membranes of proton exchange membrane fuel cells. J Test Eval 42:20120201. https://doi.org/10.1520/jte20120201
23. Osborn SJ, Hassan MK, Divoux GM, Rhoades DW, Mauritz KA, Moore RB (2007) Glass transition temperature of perfluorosulfonic acid ionomers. Macromolecules 40:3886–3890. https://doi.org/10.1021/ma062029e
24. Almeida SD, Kawano Y (1999) Thermal behavior of Nafion membranes. J Therm Anal Calorim 58:569–577. https://doi.org/10.1023/a:1010196226309
25. Kim YS, Welch CF, Hjelm RP, Mack NH, Labouriau A, Orler EB (2015) Origin of toughness in dispersion-cast Nafion membranes. Macromolecules 48:2161–2172. https://doi.org/10.1021/ma502538k

26. Bass M, Berman A, Singh A, Konovalov O, Freger V (2010) Surface structure of Nafion in vapor and liquid. J Phys Chem B 114:3784–3790. https://doi.org/10.1021/jp9113128
27. Paul DK, Karan K (2014) Conductivity and wettability changes of ultrathin Nafion films subjected to thermal annealing and liquid water exposure. J Phys Chem C 118:1828–1835. https://doi.org/10.1021/jp410510x
28. Serizawa A, Feng Z, Kawara Z (2002) Two-phase flow in microchannels. Exp Therm Fluid Sci 26:703–714. https://doi.org/10.1016/S0065-2717(01)80012-5
29. Liang Z, Zhao T, Xu C, Xu J (2007) Microscopic characterizations of membrane electrode assemblies prepared under different hot-pressing conditions. Electrochim Acta 53:894–902. https://doi.org/10.1016/j.electacta.2007.07.071
30. Sullivan J, Wronski Z, Saied S, Sielanko J (1995) Experimental and simulated XPS depth profiles of low-energy high dose nitrogen implanted into aluminium. Vacuum 46:1333–1335. https://doi.org/10.1016/0042-207X(95)00023-2
31. Gazdzicki P, Biswas I, Schulze M (2014) Methodic aspects of XPS depth profiling for investigations of fuel cell components. Surface Interface Anal 46:350–356. https://doi.org/10.1002/sia.5498
32. de Lis G A, Hitchcock AP, Berejnov V, Susac D, Stumper J, Botton GA (2016) Evaluating focused ion beam and ultramicrotome sample preparation for analytical microscopies of the cathode layer of a polymer electrolyte membrane fuel cell. J Power Sources 312:23–35. https://doi.org/10.1016/j.jpowsour.2016.02.019
33. Paul DK, Giorgi JB, Karan K (2013) Chemical and ionic conductivity degradation of ultra-thin ionomer film by X-ray beam exposure. J Electrochem Soc 160:F464. https://doi.org/10.1149/2.024306jes
34. Cumpson PJ (2001) Estimation of inelastic mean free paths for polymers and other organic materials: use of quantitative structure–property relationships. Surface Interface Anal 31:23–34. https://doi.org/10.1002/sia.948
35. Lin G, Nguyen TV (2005) Effect of thickness and hydrophobic polymer content of the gas diffusion layer on electrode flooding level in a PEMFC. J Electrochem Soc 152:A1942. https://doi.org/10.1149/1.2006487
36. Nguyen TV, Dowd RP. (2019). Methods for forming membrane electrode assemblies, United States Patent and Trademark Office, US20190044168 A1
37. Srinivasan S, Ticianelli EA, Derouin CR, Redondo A (1988) Advances in solid polymer electrolyte fuel cell technology with low platinum loading electrodes. J Power Sources 22:359–375. https://doi.org/10.1016/0378-7753(88)80030-2
38. Wood DL, Yi JS, Nguyen TV (1998) Effect of direct liquid water injection and interdigitated flow field on the performance of proton exchange membrane fuel cells. Electrochim Acta 43:3795–3809. https://doi.org/10.1016/s0013-4686(98)00139-x
39. Kuhn R, Krüger P, Kleinau S, Dawson M, Geyer J, Roscher M, Manke I, Hartnig C (2012) Dynamic fuel cell gas humidification system. Int J Hydrogen Energ 37:7702–7709. https://doi.org/10.1016/j.ijhydene.2012.01.143
40. U.S. Drive Fuel Cell Tech Team (2013) Cell component accelerated stress test and polarization curve protocols for PEM fuel cells. Office of Energy Efficiency & Renewable Energy, Washington DC
41. Cooper NJ, Smith T, Santamaria AD, Park JW (2016) Experimental optimization of parallel and interdigitated PEMFC flow-field channel geometry. Int J Hydrogen Energy 41:1213–1223. https://doi.org/10.1016/j.ijhydene.2015.11.153
42. Avcioglu GS, Ficicilar B, Bayrakceken A, Eroglu I (2015) High performance PEM fuel cell catalyst layers with hydrophobic channels. Int J Hydrogen Energy 40:7720–7731. https://doi.org/10.1016/j.ijhydene.2015.02.004
43. Wang X, Nguyen TV (2012) An experimental study of the liquid water saturation level in the cathode gas diffusion layer of a PEM fuel cell. J Power Sources 197:50–56. https://doi.org/10.1016/j.jpowsour.2011.09.036
44. Nguyen TV, Knobbe MW (2003) A liquid water management strategy for PEM fuel cell stacks. J Power Sources 114:70–79. https://doi.org/10.1016/s0378-7753(02)00591-8
45. Pivac I, Bezmalinović D, Barbir F (2018) Catalyst degradation diagnostics of proton exchange membrane fuel cells using electrochemical impedance spectroscopy. Int J Hydrogen Energy 43:13512–13520. https://doi.org/10.1016/j.ijhydene.2018.05.095

Affiliations

Regis P. Dowd Jr.[1] · Yuanchao Li[1] · Trung Van Nguyen[1]

✉ Trung Van Nguyen
cptvn@ku.edu

[1] Department of Chemical and Petroleum Engineering, The University of Kansas, 1530 W. 15th, Learned Hall Room 4132, Lawrence, KS 66045, USA